Available online at www.sciencedirect.com
SCIENCE DIRECT
Journal of volcanology and geothermal research
ELSEVIER
Journal of Volcanology and Geothermal Research 153 (2006) 125–135
www.elsevier.com/locate/jvolgeores

Fragmentation efficiency of explosive volcanic eruptions: A study of experimentally generated pyroclasts

Ulrich Kueppers *, Bettina Scheu [1], Oliver Spieler [1], Donald B. Dingwell [1]

Department für Geo- and Umweltwissenschaften, Ludwig-Maximilians-Universität München, Theresienstraße 41, 80333 München, Germany

Received 15 June 2004; accepted 17 August 2005
Available online 5 January 2006

Abstract

Products of magma fragmentation can pose a severe threat to health, infrastructure, environment, and aviation. Systematic evaluation of the mechanisms and the consequences of volcanic fragmentation is very difficult as the adjacent processes cannot be observed directly and their deposits undergo transport-related sorting. However, enhanced knowledge is required for hazard assessment and risk mitigation. Laboratory experiments on natural samples allow the precise characterization of the generated pyroclasts and open the possibility for substantial advances in the quantification of fragmentation processes. They hold the promise of precise characterization and quantification of fragmentation efficiency and its dependence on changing material properties and the physical conditions at fragmentation.

We performed a series of rapid decompression experiments on three sets of natural samples from Unzen volcano, Japan. The analysis comprised grain-size analysis and surface area measurements. The grain-size analysis is performed by dry sieving for particles larger than 250 μm and wet laser refraction for smaller particles. For all three sets of samples, the grain-size of the most abundant fraction decreases and the weight fraction of newly generated ash particles (up to 40 wt.%) increases with experimental pressure/potential energy for fragmentation. This energy can be estimated from the volume of the gas fraction and the applied pressure. The surface area was determined through Argon adsorption. The fragmentation efficiency is described by the degree of fine-particle generation. Results show that the fragmentation efficiency and the generated surface correlate positively with the applied energy.

Keywords: experimental volcanology; fragmentation efficiency; particle analysis; ash; magma; porosity; Unzen volcano

1. Introduction

Despite the lack of a generally accepted theory for the process of brittle fragmentation of magma, many influencing factors have been recognised and their contribution to volcanic eruptions elucidated. McBirney and Murase (1970) suggested that gas overpressure in bubbles and the magma's tensile strength influence the formation of pyroclastic rocks. Dingwell (1996) evaluated the viscoelastic properties of magma at fragmentation and showed that a liquid will break if the applied stress is too high to be compensated by elastic deformation and too rapidly applied to be compensated by viscous deformation. In the case of brittle fragmentation in conduits or domes, internal gas overpressure is thought to be the main driving force (Sparks, 1997; Alidibirov and Dingwell, 2000). Taddeucci et al. (2004) performed SEM analysis of natural ash particles (2001 Etna

* Corresponding author. Tel.: +49 89 21804221; fax: +49 89 21804176.
E-mail address: ulli@min.uni-muenchen.de (U. Kueppers).
[1] Tel.: +49 89 21804221; fax: +49 89 21804176.

0377-0273/$ - see front matter © 2005 Elsevier B.V. All rights reserved.
doi:10.1016/j.jvolgeores.2005.08.006

Table 1
Overview of the important physical properties of the three used sample suites. The open and closed porosity are determined with Helium Pycnometry, the fragmentation threshold was evaluated with rapid decompression experiments. The specific sample surface is determined via Argon adsorption. The "inner" surface is the total measured surface minus the surface represented by bottom, top, and wall of the cylinder. The small difference between these two values did not allow performing any correction when calculating the total surface increase (%)

Sample name	Weight (g)	Open porosity (%)	Range in porosity	Closed porosity (%)	Threshold (MPa)	Specific sample surface (m^2/g)	Total cylinder surface (m^2)
MUZ A	70	7.0	±1.5	0.4	22.5	0.0247	1.744
MUZ C	59	20.5	±1.0	0.9	5.8	0.0329	1.951
MUZ F	47	35.5	±1.0	2.0	3.5	0.0419	1.984

eruption) and experimentally generated pyroclasts from fragmentation experiments on samples erupted during this activity period. All particles showed sharp edges and rough fracture surfaces. They concluded that the magma mainly fragmented in a brittle way without signs of ductile fragmentation and thereby demonstrated the reproducibility of the brittle fragmentation process by rapid decompression experiments in the fragmentation bomb (Alidibirov and Dingwell, 1996). Experiments at 850 °C on samples from several volcanoes revealed an inverse, nonlinear dependency of the overpressure required for full fragmentation of the used samples with open porosity (Spieler et al., 2004). For Unzen samples, this fragmentation threshold has additionally been determined at room temperature and the experimental temperature was not observed to influence the onset of fragmentation significantly.

In the light of the continued need for information on ash generation and its associated energy conversion (Zimanowski et al., 2003), we performed further hot fragmentation experiments at initial overpressure conditions above the fragmentation threshold (Fig. 3). We show the results of grain-size and surface analysis of experimentally generated pyroclasts and discuss the parameters that influence the generation of fine particles.

2. Sample description

All samples were collected in 2001 from block-and-ash flow (BAF) deposits of the 1990–1995 Unzen eruption (Table 1). Extensive fieldwork revealed that the sample's physical properties (e.g. porosity, crystallinity) did not change measurably during the BAF transport or after deposition (Kueppers et al., 2005). Importantly, the collected samples have not been subject to hydrothermal alteration as samples from the dome would have been after a long period of time emplaced over the vent.

We drilled cylinders (d=25 mm, l=60 mm) from three sets of dome-forming samples for which the porosity was measured by Helium Pycnometry. The porosities provided here represent values of open porosity averaged from at least 20 measurements per sample set. The 7.0 vol.% porosity samples (MUZ A) represent the densest rock type we found, the 20.5 vol.% porosity samples (MUZ C) the most abundant rock variety and the 35.5 vol.% samples (MUZ F) the most porous rocks of the dome. Bread-crust bombs from vulcanian explo-

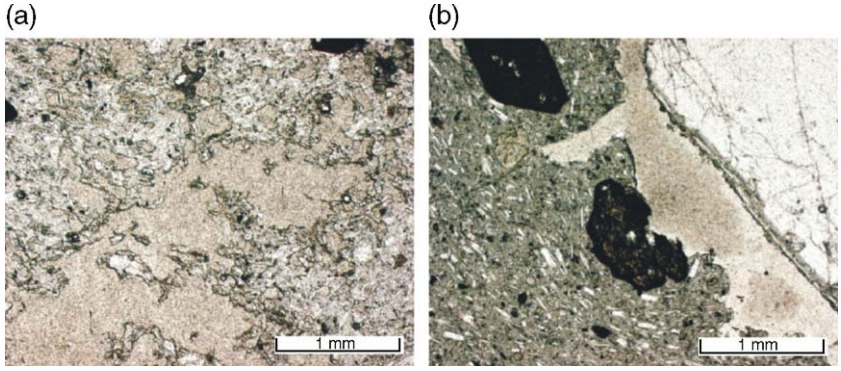

Fig. 1. Microscope photographs of Unzen samples. (a) Image of porous sample showing the high number of irregularly shaped bubbles. (b) Image of dense sample showing the flow alignment of phenocrysts and microlites. The bubble number density is low and bubbles often touch the phenocrysts.

sions in June 1991 exhibit the highest overall value of porosity (as high as 53.0 vol.%) but have not been used for this study. The closed porosity in the lava samples was found to be generally below 2.5 vol.%. Due to its low percentage and the fact that these pores are not pressurized with Argon during the experiments, it has only a negligible influence on the results.

Petrographic studies reveal a nearly constant ratio of phenocrysts to matrix. These phenocrysts (mostly plagioclase and hornblende with minor biotite and quartz) are typically up to 6 mm long (Nakada and Motomura, 1999), some exceptional large ones measure up to 20 mm length. The abundance of the phenocrysts ranges from 23 to 28 vol.%. We observed a flow alignment of phenocrysts and microlites parallel to bubble elongation within a range of approximately 20°. The microlite content of MUZ A samples is slightly higher than for MUZ C and MUZ F samples. Due to the high content of microlites, the shape of the bubbles is irregular with rough bubble walls (Fig. 1a). In dense samples, bubbles often touch large phenocrysts (Fig. 1b). The bubble number density is much higher in the porous samples. All samples exhibit usually non-spherical bubbles with microlites frequently deforming the bubble walls. Their shapes may be the products of syn-ascent shearing and/or partial bubble collapse upon effective degassing.

3. Fragmentation experiments and sample preparation

We performed hot fragmentation experiments (850 °C) in the fragmentation bomb, a device that permits the simulation of volcanic conditions in terms of temperature, gas overpressure and rate of decompression. It thereby allows quantifying the effect of porosity upon magma fragmentation and its efficiency during rapid decompression. The modified experimental set-up consists of three main units (Spieler et al., 2004):

(1) A low-pressure tank (inner dimensions $d = 40$ cm, $l = 300$ cm) at ambient pressure that represents the atmosphere and acts as pyroclast sampling container.
(2) A pressurization system with three diaphragms that open at a relative pressure differential.
(3) An externally heated pressure vessel containing the cylindrical specimens separated from the low-

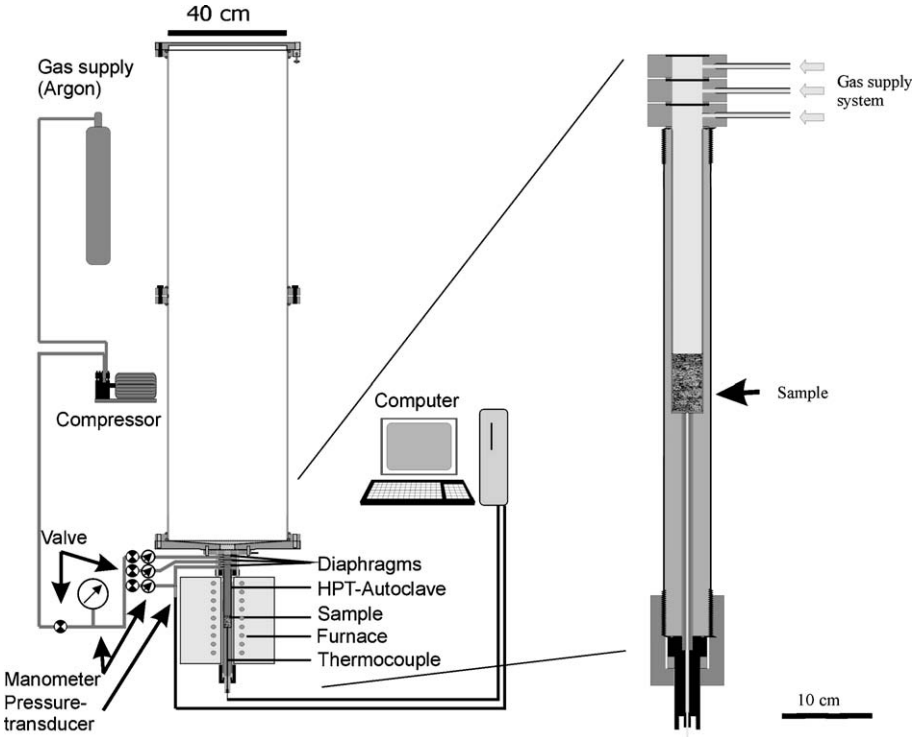

Fig. 2. Experimental setup of the fragmentation bomb. The large tank is at ambient pressure and collects the pyroclasts. A set of up to three diaphragms maintains the pressure differential to the externally heated, high pressure autoclave where the sample is placed.

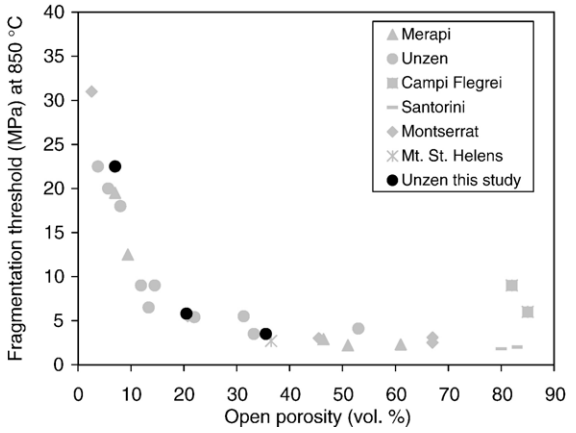

Fig. 3. Fragmentation threshold vs. sample porosity. Porosity exhibits strong influence on the fragmentation threshold (modified from Spieler et al., 2004). All experiments in this study have been performed above the respective fragmentation threshold values indicated by this diagram.

pressure tank by the diaphragms (2). The sample is located at the base of the high-P chamber (d=2.8 cm, l=24 cm).

This set-up (Fig. 2) allows precise and reproducible pressurization of the sample. As it is gastight in its entirety, the loss of fine particles is minimized. Heating is performed at a rate of ≈15 K/min to 850 °C. In order to avoid heating-induced changes in the physical properties of the sample, we pressurize the sample with 2 MPa of Argon before heating. At the final experimental temperature, the sample is slowly pressurized to the desired experimental pressure. As seen from earlier experiments (Spieler et al., 2004), the fragmentation primarily depends on the open porosity of the specific sample as this defines how much energy in form of pressurized gas can be stored inside the sample. Accordingly, all experiments in this study are performed at initial pressure values above the threshold (Fig. 3). The samples are completely fragmented and "erupted" into the low-pressure tank. After the experiment, we allow at least 2 h for cooling and particle settling. This time span was required for cooling of the high-T section and settling of the fine ash particles according to Stokes' Law.

4. Pyroclast analysis

We use distilled water at 8.5 MPa to rinse the low-pressure tank. The water–pyroclast mixture flows through a 250-μm sieve and is thereby separated into a coarse and a fine fraction. Both fractions are dried and weighed. Sieving is performed at half-Φ steps ($\Phi=-\log_2 d$, with d=particle diameter in mm, e.g. Cas and Wright, 1988 or literature cited therein). Analysis of the coarse fraction comprises weighing, dry sieving, and surface analysis. Analysis of the fine fraction comprises weighing, surface analysis, wet laser refraction, and dry sieving after the laser refraction.

4.1. Sieving

The coarse fraction (x>250 μm) is sieved (dry) at half-Φ steps. Sieving duration was approximately 10 s per sieve class for particles ≥2 mm and approximately 20 s per sieve class for smaller particles. This results in a maximum total sieving duration of 180 s for the smallest particles of this fraction. Repetitive sieving confirms the high accuracy of this sieving duration. The weight of all particles smaller than 250 μm after the sieving (sieving abrasion) is generally below 0.7% of the sample weight.

After the laser refraction analysis, the fine particles were dried and particles larger than 90 μm were sieved at 2.5, 3, and 3.5 Φ. This allowed for comparison of the laser refraction and sieving data. As the laser refraction method to grain-size analysis of natural ash particles from Unzen volcano was found to be sufficiently precise, it was now possible to combine sieving (wt.%) and laser refraction (vol.%) data to a coherent grain-size distribution plot. For that, the laser refraction data were recalculated to wt.%.

4.2. Surface analysis

Surface analysis was performed at cryogenic conditions (77 K) via Argon adsorption in a Micromeritics Gemini 2375 and the specific surface area was determined using the BET method (Brunauer et al., 1938). The technique is a relative measurement between two glass tubes, an empty reference tube and a tube with the sample therein. The different volumes of these tubes were determined using Helium 5.0 that is not adsorbed at the experimental conditions. After another evacuation procedure, Argon 5.0 was added in both tubes. The gas was assumed to be adsorbed as a monolayer on any free surface (i.e. all outer sample surfaces plus any bubble/fracture surface of the open pore space). Additional Argon has been dispensed into the sample tube until no further pressure reduction due to adsorption had been taking place. No adsorption is supposed to take place on ideal glass surfaces. From the amount of Argon adsorbed, the tube volumes, and

the sample weight, the specific surface area (m^2/g) represented by the sample is obtained (Kueppers, 2005 and literature cited therein).

Surface analysis by Argon adsorption is very time-consuming compared to theoretical models (e.g. Koptsik et al., 2003). However, despite recent improvements, models still underestimate the surface areas actually measured by as much as two orders of magnitude (Riley et al., 2003). The discrepancy between measured and modelled values of surface area comes from simplified geometrical assumptions in these models. Experimentally derived pyroclasts from natural magmas are irregular in shape and heterogeneous and thus deviate in their surfaces from simple geometric particles.

Several cylinders of each set of samples have been measured to determine the pre-fragmentation surface. The specific surface area before fragmentation (As_{spec} [m^2/g]) multiplied by the weight of the cylinder (m_{cyl} [g]) yields the pre-fragmentation cylinder surface (As_{cyl} [m^2]).

$$As_{cyl} = As_{spec} * m_{cyl} \quad (1)$$

At the beginning of the pyroclast analysis, we tempted to quantify the surface increase represented by each size class separately. It became clear very quickly, that the surface area represented by the particles of a single sieve class from a single sample is below the minimum detectable limit (0.1 m^2). Therefore, we accumulated the particles of several sieve classes to fulfil measuring requirements. Surface analysis was accordingly performed for four size groups:

(1) $x < 250$ μm (I),
(2) $250 < x < 710$ μm (II),
(3) $710 < x < 2000$ μm (III), and
(4) $x > 2000$ μm (IV).

Size group I comprises all fine particles separated during the rinsing process. Size groups II and III comprise three sieve classes each. The surface area of each size group was calculated according to Eq. (1). Analysis of the particles larger than 2 mm (size group IV) showed that the specific surface area represented by these particles was in the range of the specific pre-fragmentation surface area of the corresponding cylinder. As a consequence by way of simplification, we assumed that this size group does not contribute effectively to the surface increase and it was only measured for few samples to confirm this assumption.

The total pyroclasts surface is calculated by summing up the surfaces of each size group. For size group IV, the specific surface area value of the respective cylinder was used:

$$\begin{aligned} As_{pyroclasts} = {} & As_{spec}(I) * m(I) + As_{spec}(II) * m(II) \\ & + As_{spec}(III) * m(III) \\ & + As_{spec}(cyl) * m(IV). \end{aligned} \quad (2)$$

The increase in surface area was evaluated by comparing pre- and post-fragmentation values.

$$\Delta As = \left[\frac{As_{pyroclast} - As_{cyl}}{As_{cyl}} * 100 \right]. \quad (3)$$

4.3. Laser refraction analysis

Grain-size analysis was performed by laser refraction technique using a Coulter LS230 (measuring range 0.375–2000 μm, wave length 750 nm). The laser beam is refracted at the surface of the individual particles. The degree of refraction is related to the particle size and the angle of refraction increases with decreasing particle size. The intensity of the light refracted with a certain angle depends on the proportion of the particle size in question.

In this study, 250 μm was chosen as grain-size boundary between sieving and laser refraction analysis. As the sample amount for the laser refraction was too high to be measured in a single run, it was split into sub-fractions of approximately 0.1 g each. Each sub-fraction was measured independently. The data have been evaluated with the Fraunhofer Theory (Weiner, 1984). The results of all sub-fractions of one sample were assessed based on their weight and the result for the complete sample (vol.%) was calculated. After the laser refraction, the sample was dried and particles larger than 90 μm were sieved (2.5, 3, and 3.5 Φ) to check the applicability of the laser refraction method to grain-size analysis of natural ash particles.

4.4. SEM analysis

Scanning Electron Microscopy analysis was performed on pyroclasts of variable grain size. Although all particles are derived from experiments at 850 °C (i.e. above Tg), no particle was found that exhibited signs of post-fragmentation surface changes by surface tension.

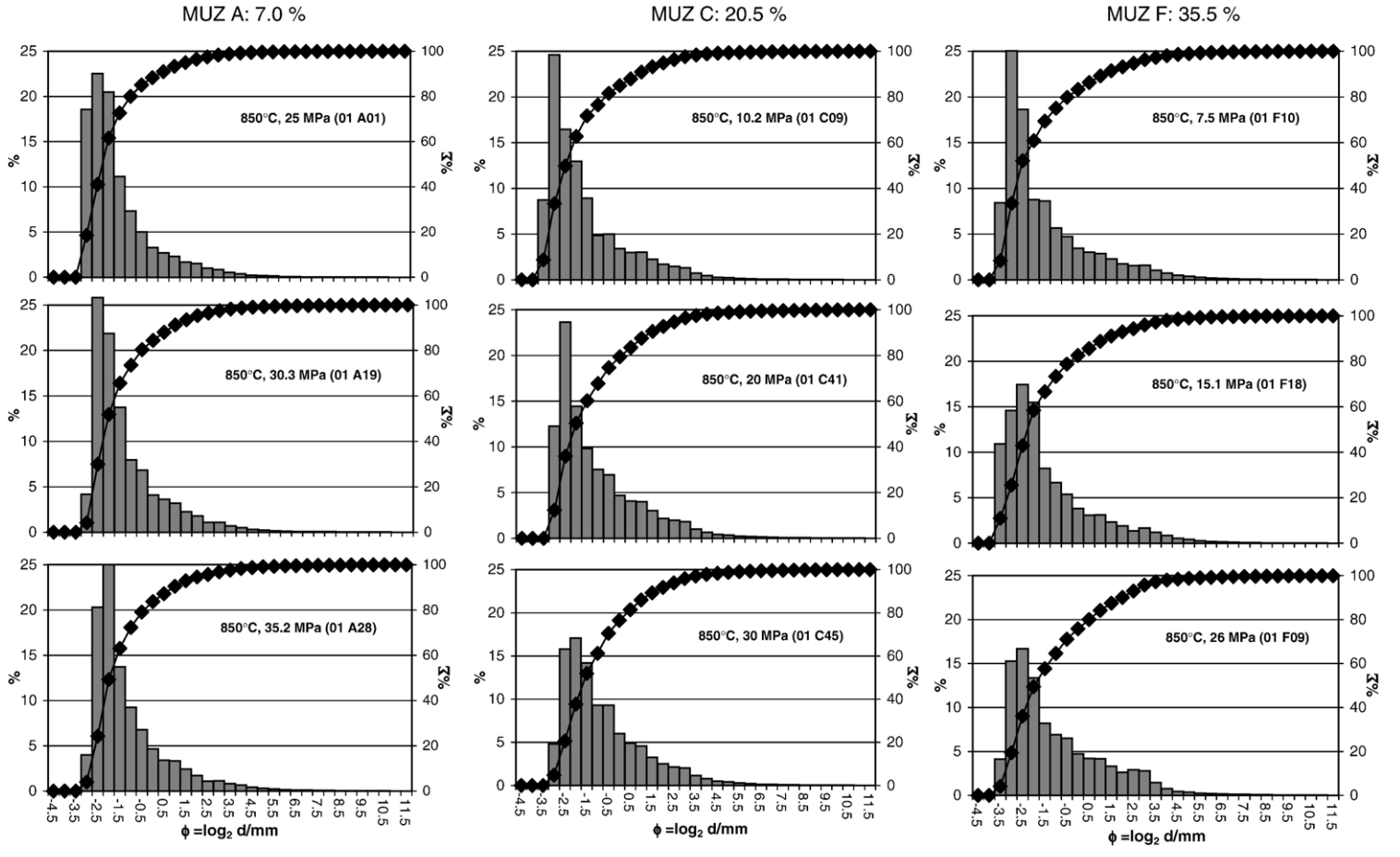

Fig. 4. Grain-size distribution plot showing the relation of wt.% and particle size (Φ, $\Phi = -\log_2 d$ with d = particle diameter in mm) of rapid decompression experiments at 850 °C for three different pressure steps for 7.0 vol.% (MUZ A, left column), 20.5 vol.% (MUZ C, middle column) and 35.5 vol.% porosity sample (MUZ F, right column). MUZ stands for Mt. Unzen, the letters correspond to sample names given in the field based on their density (Kueppers et al., 2005). The height of the grey columns represents the wt.%-values for each sieving class. The grain size is decreasing to the right in each plot. The curve of black diamonds shows the sum curve of the weight fractions. The grain-size reduction of the coarse pyroclasts with increasing pressure is clearly visible.

5. Results

Our data analysis was twofold: We evaluated the grain-size distribution of the experimental pyroclasts as a function of porosity and applied pressure, and the increase in surface area as a function of particle size and applied energy (Figs. 4–7). The results of laser refraction technique and post-laser refraction sieving (dry) differ by less than 0.5 wt.% based on the total sample weight and demonstrate the applicability of the laser refraction method for the grain-size analysis of pyroclasts from natural samples that are irregularly shaped and exhibit varying refraction indices. The laser refraction data (vol.%) have been converted to wt.% and assessed to half-Φ steps. In this way, these data can be combined with the sieving data and form a complete grain-size plot. All total grain-size plots from one set of samples exhibit the following features (Fig. 4): (1) a non-Gaussian particle size distribution, (2) decreasing grain-size of the most abundant fraction with increasing experimental pressure, and (3) increasing weight fraction of ash sized particles with increasing experimental pressure. The latter fact turns out even more clearly in Fig. 5. Although all three data sets exhibit a large scatter, the positive correlation is beyond question. Furthermore, it can be stated that for any applied pressure, the amount of ash particles produced increases with the samples' porosity as this is directly linked with the potential energy for fragmentation (PEF). It can be estimated from sample volume (V_{cyl} [m^3]), its porosity (θ, dimensionless), and the applied pressure (ΔP [Pa]), and may be approximated as:

$$\mathrm{PEF}: = \theta * V_{cyl} * \Delta P. \quad (4)$$

An investigation of all experimental pyroclasts according to Schleyer (1987) revealed that the grain-size distributions follow a Rosin-distribution. Accordingly, the appropriate parameter to express the overall grain-size reduction (i.e. the fragmentation efficiency) is defined as:

$$\text{Mean diameter} = (\Phi_{18.4} + \Phi_{36.79} + \Phi_{68.4})/3.$$

The evaluated values for all samples are in the range of 0 and 1.5. Large Φ-values represent large mean particle sizes. Fig. 6 shows the mean diameter in relation to the PEF. It becomes apparent that higher values of energy must be applied for samples with a higher porosity in order to achieve a value of mean diameter comparable to the one of the dense samples. The fragmentation of low porosity samples was more efficient than that of high porosity samples as the applied pressure was effectively reduced by permeable gas flow

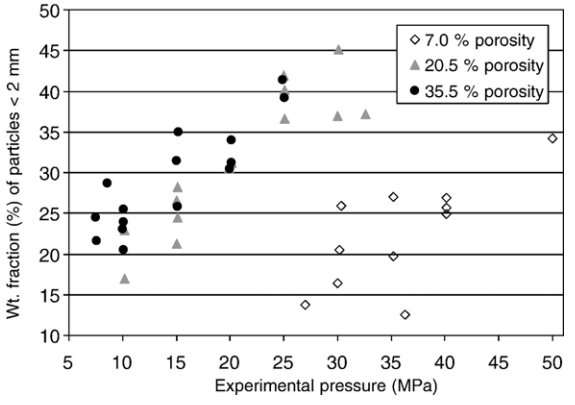

Fig. 5. Plot of the weight fraction of particles smaller than 2 mm vs. the applied pressure (MPa). All three data sets show a positive correlation. The large scatter is probably due to sample heterogeneities.

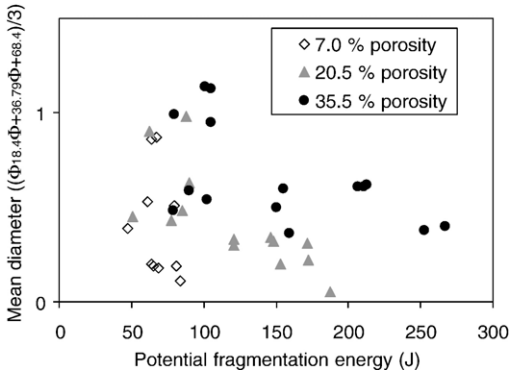

Fig. 6. Plot of mean diameter vs. potential energy. Large mean diameter values represent large particles. The data from MUZ A samples show a large scatter but are in agreement with the general trend represented by the other data sets. Mean diameter values for MUZ C samples are generally slightly lower compared to MUZ F samples.

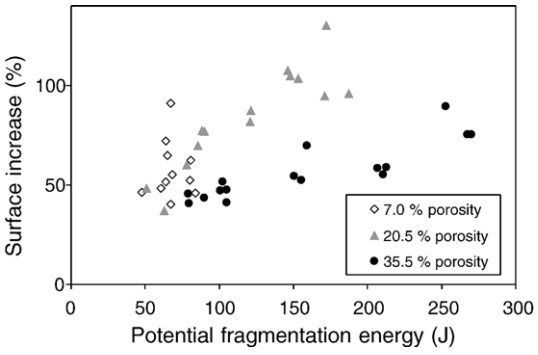

Fig. 7. A plot of potential energy for fragmentation (PEF) against the surface increase (%) clearly shows a positive correlation for MUZ C and MUZ F samples. The dense samples show no clear correlation. It becomes apparent that the surface increase is higher for MUZ C samples than for MUZ F samples. We speculate that this is related to a decrease of bubble wall thickness with increasing porosity.

Table 2
Results from surface analysis measurements for the three size groups for the 7.0 (MUZ A), 20.5 (MUZ C), and 35.5 vol.% porosity samples (MUZ F). For details on the calculation of the surface increase (%), please refer to the surface analysis section in the pyroclast analysis chapter

Sample name	$P_{applied}$ (MPa)	m_{cyl} (g)	Open porosity (%)	Energy (J)	As_{spec} (m^2/g)	Pre-fragmentation surface (m^2)	Size group I			Size group II			Size group III			Surface increase (%)
							$x<250$ (g)	wt.%	As_{spec} (m^2/g)	$250<x<710$ (g)	wt.%	As_{spec} (m^2/g)	$710<x<1400$ (g)	wt.%	As_{spec} (m^2/g)	
MUZ 2001 A26	27.0	69.7760	8.11	63.9	0.0255	1.7769	1.9923	2.86	0.2396	2.7245	3.90	0.1074	4.8900	7.01	0.0300	37.80
MUZ 2001 A33	30.0	72.8515	5.39	47.6	0.0238	1.7363	2.3144	3.18	0.1556	3.5342	4.85	0.0657	6.0833	8.35	0.0349	29.95
MUZ 2001 A21	30.2	70.5884	6.90	60.9	0.0247	1.7464	2.3361	3.31	0.1581	3.9913	5.65	0.0441	8.1786	11.59	0.0365	27.45
MUZ 2001 A19	30.3	70.3170	7.26	64.1	0.0250	1.7548	2.9248	4.16	0.1969	5.0710	7.21	0.0535	10.1877	14.49	0.0413	46.14
MUZ 2001 A27	35.2	69.6333	8.18	83.9	0.0255	1.7762	2.3542	3.38	0.1777	3.8850	5.58	0.0434	7.4838	10.75	0.0305	26.05
MUZ 2001 A28	35.2	69.8255	7.86	80.7	0.0253	1.7677	3.2828	4.70	0.1335	5.2200	7.48	0.0489	10.3571	14.83	0.0398	35.47
MUZ 2001 A24	36.3	71.3758	6.32	67.1	0.0244	1.7410	1.6625	2.33	0.1976	2.6100	3.66	0.0631	4.6568	6.52	0.0447	27.67
MUZ 2001 A32	40.1	71.5525	5.51	64.9	0.0239	1.7105	3.2049	4.48	0.1429	5.3778	7.52	0.0524	10.6375	14.87	0.0351	37.95
MUZ 2001 A29	40.1	72.2315	5.80	68.4	0.0241	1.7393	3.5021	4.85	0.1467	5.1595	7.14	0.0363	9.9297	13.75	0.0259	29.33
MUZ 2001 A30	40.1	70.7337	6.78	80.0	0.0247	1.7449	2.4989	3.53	0.1420	5.1595	7.29	0.0477	9.9297	14.04	0.0318	27.61
MUZ 2001 A31	50.0	72.4672	4.60	67.1	0.0234	1.6928	4.3300	5.98	0.1600	6.8740	9.49	0.0315	13.5670	18.72	0.0466	56.86
			7.0		0.0246	1.7443			0.1611			0.0487			0.0361	
MUZ 2001 C09	10.2	51.0530	20.08	51.0	0.0326	1.6668	2.3673	4.64	0.1590	3.5504	6.95	0.0542	5.7962	11.35	0.0410	25.28
MUZ 2001 C22	10.2	58.5668	21.29	62.8	0.0334	1.9546	1.9780	3.38	0.1619	2.8658	4.89	0.0655	5.0787	8.67	0.0421	19.61
MUZ 2001 C32	15.0	50.3824	20.90	77.8	0.0331	1.6697	2.2285	4.42	0.1527	3.0543	6.06	0.0942	5.4212	10.76	0.0698	38.75
MUZ 2001 C44	15.0	58.4138	20.50	89.8	0.0329	1.9218	3.2690	5.60	0.1986	4.3724	7.49	0.0803	7.8524	13.44	0.0616	50.33
MUZ 2001 C01	15.1	59.3028	20.19	88.1	0.0327	1.9400	2.3195	3.91	0.1664	5.5919	9.43	0.0908	8.8055	14.85	0.0693	49.12
MUZ 2001 C46	15.1	60.5848	19.35	85.4	0.0322	1.9514	3.1253	5.16	0.1865	4.2089	6.95	0.0777	7.4680	12.33	0.0605	45.01
MUZ 2001 C41	19.9	59.3698	20.79	120.7	0.0331	1.9636	3.4148	5.75	0.1804	5.4465	9.17	0.0674	9.2716	15.62	0.0671	50.80
MUZ 2001 C38	20.1	59.1292	20.71	121.1	0.0330	1.9528	3.7526	6.35	0.1756	5.7017	9.64	0.0779	8.9956	15.21	0.0677	56.00
MUZ 2001 C42	25.0	59.0422	21.06	153.1	0.0332	1.9623	4.5814	7.76	0.1567	7.0669	11.97	0.0595	13.1013	22.19	0.0683	61.24
MUZ 2001 C43	25.1	59.7170	20.25	148.0	0.0328	1.9557	4.1520	6.95	0.1873	6.2330	10.44	0.0667	11.4650	19.20	0.0749	68.00
MUZ 2001 C39	25.1	59.8408	19.99	146.0	0.0326	1.9505	4.5673	7.63	0.1792	7.0045	11.71	0.0671	12.4657	20.83	0.0653	67.20
MUZ 2001 C45	30.0	60.5014	19.54	171.4	0.0323	1.9556	3.9815	6.58	0.1692	6.2350	10.31	0.0687	12.1566	20.09	0.0617	57.23
MUZ 2001 C40	30.1	60.2772	19.59	172.1	0.0324	1.9502	5.6844	9.43	0.1700	7.6436	12.68	0.0572	13.8477	22.97	0.0823	84.91
			20.50		0.0328	1.9514			0.1739			0.0711			0.0638	

Table 2 (*continued*)

Sample name	$P_{applied}$ (MPa)	m_{cyl} (g)	Open porosity (%)	Energy (J)	As_{spec} (m^2/g)	Pre-fragmentation surface (m^2)	Size group I			Size group II			Size group III			Surface increase (%)
							$x<250$ (g)	wt.%	As_{spec} (m^2/g)	$250<x<710$ (g)	wt.%	As_{spec} (m^2/g)	$710<x<1400$ (g)	wt.%	As_{spec} (m^2/g)	
MUZ 2001 F10	7.5	47.0880	36.06	79.1	0.0422	1.9888	3.0603	6.50	0.1449	3.2149	6.83	0.0611	5.2665	11.18	0.0503	20.67
MUZ 2001 F08	7.6	47.2526	35.85	79.7	0.0421	1.9898	2.4828	5.25	0.1296	2.8947	6.13	0.0717	4.8289	10.22	0.0590	18.84
MUZ 2001 F21	8.6	47.4114	35.64	90.0	0.0420	1.9905	3.9005	8.23	0.0885	3.7631	7.94	0.0627	5.9566	12.56	0.0487	14.62
MUZ 2001 F12	10.1	47.2564	35.62	105.3	0.0420	1.9834	3.1734	6.72	0.1448	3.2246	6.82	0.0654	4.9068	10.38	0.0555	23.08
MUZ 2001 F13	10.1	47.6276	34.55	102.1	0.0413	1.9684	3.3827	7.10	0.1659	3.4005	7.14	0.0596	5.3688	11.27	0.0472	25.77
MUZ 2001 F16	10.1	47.4890	35.43	104.9	0.0419	1.9878	2.4503	5.16	0.1678	2.7583	5.81	0.0576	4.5338	9.55	0.0548	20.39
MUZ 2001 F17	10.0	48.5094	34.23	100.6	0.0411	1.9956	2.8576	5.89	0.1689	3.1031	6.40	0.0549	5.2026	10.72	0.0552	23.68
MUZ 2001 F18	15.1	47.8340	34.33	150.4	0.0412	1.9707	3.0041	6.28	0.1874	3.4974	7.31	0.0607	5.8624	12.26	0.0505	28.28
MUZ 2001 F19	15.2	46.6414	36.05	159.3	0.0422	1.9697	4.5497	9.75	0.1655	4.5519	9.76	0.0547	7.2352	15.51	0.0520	34.55
MUZ 2001 F20	15.0	47.1762	35.54	155.2	0.0419	1.9778	4.0531	8.59	0.1288	3.9998	8.48	0.0546	6.7881	14.39	0.0439	20.63
MUZ 2001 F01	20.0	47.2460	35.93	210.7	0.0422	1.9918	3.6589	7.74	0.1619	4.2448	8.98	0.0584	6.4738	13.70	0.0405	24.47
MUZ 2001 F02	20.1	47.0156	36.19	213.0	0.0423	1.9894	4.1664	8.86	0.1421	4.6040	9.79	0.0504	7.2128	15.34	0.0481	24.53
MUZ 2001 F05	20.1	47.5074	35.22	206.8	0.0417	1.9826	3.6797	7.75	0.1665	4.2842	9.02	0.0558	6.8398	14.40	0.0446	26.69
MUZ 2001 F06	25.1	46.7618	36.36	267.4	0.0424	1.9834	4.8863	10.45	0.1611	5.2675	11.26	0.0464	8.1739	17.48	0.0568	35.90
MUZ 2001 F07	24.9	47.9322	34.76	252.7	0.0415	1.9871	5.4433	11.36	0.1736	5.5919	11.67	0.0531	8.8055	18.37	0.0607	47.51
MUZ 2001 F09	26.0	47.2388	35.55	270.3	0.0419	1.9807	4.4224	9.36	0.1713	4.7439	10.04	0.0514	7.2688	15.39	0.0678	40.32
average values			35.50		0.0419	1.9836			0.1543			0.0574			0.0522	

(Mueller et al., 2005). The increase in surface area was evaluated as described above by comparing pre- and post-fragmentation values. The specific surface area (As_{spec}) of the sample cylinders ranges, depending on open porosity, from 0.020 to 0.045 m^2/g. The mean pre-fragmentation surface area (As_{cyl}) of the analysed sample sets is in the order of 1.7 to 2.0 m^2 (Table 1). It is noteworthy that even large differences in open porosity do not show a large impact on the represented free surface. The experimental pyroclasts have been measured in three size groups and the results show that the specific surface area (m^2/g) increases with decreasing particle size. For MUZ A samples for example, As_{spec} is 0.0361, 0.0487, and 0.1611 m^2/g for size groups I, II, and III, respectively (Table 2). All values are averaged for the given sample set. The total surface increase represented by the pyroclasts of one sample is achieved as described above. The surface increase is positively correlated with the PEF. Results from experiments with dense samples show large scatter but the trend is clearly visible for samples with a higher porosity (Fig. 7). It should be highlighted that the newly generated surface is approximately twice as high for MUZ C samples compared to MUZ F samples.

6. Interpretation

Our experimental set-up allows for a complete sampling of pyroclasts generated during gas-overpressure-driven fragmentation under well-constrained conditions. As the experimental pyroclasts underwent only negligible transportation-related sorting, the resultant grain-size distributions will, as a rule, differ from grain-size distributions of natural deposits.

Brittle magma fragmentation occurs when the stress exerted by gas on the bubble walls cannot be dissipated by viscous deformation and exceeds the tensile strength (Dingwell, 1996). Porous samples are characterized by very high bubble number densities, thus relatively thin bubble walls. In general, thinner bubble walls withstand less pressure differential. However, it is well known from fibre drawing tests (Dingwell and Webb, 1989) showed that below a certain critical thickness, high surface tension values may lead to an increase in strength. SEM investigations of natural ash particles and pyroclasts produced during fragmentation experiments as described above did not reveal any sign for post-fragmentation changes in surface shapes (Taddeucci et al., 2004). We therefore choose to not take into account the potential contribution of ductile fragmentation for the interpretation of our data. The effects of increasing pressure on the generation of pyroclasts are shown. All three sets of samples show a shift of the most abundant grain-size fraction to a smaller size (Fig. 4) and increasing weight fraction of the ash particles (Fig. 5) with increasing pressure. For a given pressure, the amount of ash particles produced is highest for MUZ F samples. The large scatter within each data set (Fig. 5) may derive from locally restricted heterogeneities of the natural samples. The data points of MUZ C and MUZ F samples are very similar. A plot of PEF vs. the mean diameter (Fig. 6) clearly shows that it is the applied pressure in combination with the open porosity that control the pyroclast generation.

To achieve a comparable energy value, higher values of overpressure have to be applied in samples with a lower open porosity. Surface analysis of cylinders revealed very similar values for all three used sample sets (Table 1). As a consequence, the pressure/surface ratio is higher with lower porosity. Although bubble walls do generally become thicker with decreasing porosity, the fragmentation efficiency is highest for MUZ C samples for any value of PEF. Beside the pressure/surface ratio, pressure loss through permeable gas flow may be another reason for the higher fragmentation efficiency of MUZ C than MUZ F samples as it may effectively reduce the overpressure before and during fragmentation. Mueller et al. (2005) investigated cold Unzen samples with the same dimensions as used for this study. Their study reveals that permeability is increasing with porosity. In this study, experiments have been performed at pressures as high as 50 MPa as the fragmentation experiments intended to simulate gas-overpressure-driven eruption within the conduit or the dome. Further experiments with dome-forming samples of approximately 50 vol.% open porosity would complete the picture of the relationship of fragmentation efficiency and the combination of applied pressure and open porosity. Due to their vulcanian origin, the Unzen bread-crust bombs have not been used for this purpose here.

In addition to the grain-size analysis, the fragmentation efficiency was evaluated as a function of surface increase (%). This quantifies the amount of new fracture surfaces generated by brittle fragmentation upon rapid decompression. Fig. 7 shows a plot of surface increase (%) vs. potential energy for fragmentation. Here, the trend indicated by Fig. 6 becomes even more striking. The amount of new surface represented by MUZ C samples is approximately twice as high as for MUZ F samples. We speculate that this is related to a decrease of bubble wall thickness with increasing porosity. We have to bear in mind that a single bubble wall might break several times at high overpressures.

However, most fracture surfaces in MUZ F samples are likely to be smaller than in MUZ C samples and will therefore not contribute as much to the total surface increase. Accordingly, any bubble wall break-up in MUZ C samples will represent more newly formed surface than it would in MUZ F samples.

7. Summary

We have performed hot fragmentation experiments on three sets of Unzen samples to investigate the influence of open porosity in combination with applied pressure on the fragmentation behaviour and pyroclast generation. The grain-size distribution was analysed by dry sieving for particles >250 μm and laser refraction of the suspended particles smaller than 250 μm. Laser refraction–though designed for spherical particles–was found to be applicable to the size analysis of pyroclasts from natural samples. The increase in surface area has been evaluated by Argon adsorption of pre-fragmentation cylinders and post-fragmentation pyroclasts. Our results show that fragmentation efficiency depends on the potential energy for fragmentation (PEF) stored in the samples that can be estimated from the porosity and the applied pressure. Grain-size and surface analysis data for the dense samples (MUZ A) generally exhibit a large scatter but the mean (MUZ C) and highly porous samples (MUZ F) show concordant trends. At a constant pressure, the weight fraction of experimentally derived ash particles is highest for the most porous samples. Data from each sample set indicate increasing amounts of ash particles with increasing pressure. At a comparable value of PEF, the average grain-size is smaller for MUZ C samples indicating a more efficient fragmentation. The increase in surface is approximately twice as high for MUZ C samples compared to MUZ F samples. We speculate that this has two reasons: (1) higher pressure/surface ratio with decreasing porosity and (2) decreasing bubble wall thickness with increasing porosity.

Acknowledgements

The work was funded by the EU (MULTIMO) and DFG (DI 431/20-1). We thank Joachim Gottsmann for field assistance during the 2000 field campaign, and Yan Lavallée and Jacopo Taddeucci for helpful comments. We are thankful for review comments by Mie Ichihara, Oded Navon, and an anonymous reviewer.

References

Alidibirov, M., Dingwell, D.B., 1996. An experimental facility for investigation of magma fragmentation by rapid decompression. Bull. Volcanol. 58, 411–416.

Alidibirov, M., Dingwell, D.B., 2000. Three fragmentation mechanisms for highly viscous magma under rapid decompression. J. Volcanol. Geotherm. Res. 100, 413–421.

Brunauer, S., Emmett, P.H., Teller, E.J., 1938. Adsorption of gases in multimolecular layer. Am. Chem. Soc. 60, 309.

Cas, R.A.F., Wright, J.V., 1988. Volcanic Successions: Modern and Ancient. Chapman and Hall, 528 pp.

Dingwell, D.B., 1996. Volcanic dilemma: blow or flow? Science 273, 1054–1055.

Dingwell, D.B., Webb, S.L., 1989. Structural relaxation in silicate melts and non-Newtonian melt rheology in igneous processes. Phys. Chem. Miner. 16, 508–516.

Koptsik, S., Strand, L., Clarke, N., 2003. On the calculation of the surface area of different soil size fractions. Appl. Geochem. 18, 629–651.

Kueppers, U, 2005. Nature and efficiency of pyroclast formation from porous magma: Insights from field investigations and laboratory experiments. PhD thesis, University of Munich, Germany, http://edoc.ub.uni-muenchen.de/view/subjects/fak20.html.

Kueppers, U., Scheu, B., Spieler, O., Dingwell, D.B., 2005. Field-based density measurements as tool to identify pre-eruption dome structure: set-up and first results from Unzen volcano, Japan. J. Volcanol. Geotherm. Res. 141, 65–75.

McBirney, A.R., Murase, T., 1970. Factors governing the formation of pyroclastic rocks. Bull. Volcanol. 34, 372–384.

Mueller, S., Melnik, O., Spieler, O., Scheu, B., Dingwell, D.B., 2005. Permeability and degassing of dome lavas undergoing rapid decompression: an experimental determination. Bull. Volcanol. 67 (6), 526–538.

Nakada, S., Motomura, Y., 1999. Petrology of the 1991–1995 eruption at Unzen: effusion pulsation and groundmass crystallisation. J. Volcanol. Geotherm. Res. 89, 173–196.

Riley, C.M., Rose, W.I., Bluth, G.J.S., 2003. Quantitative shape measurements of distal volcanic ash. J. Geophys. Res. 108 (B10), 2504, doi:10.1029/2001JB000818.

Schleyer, R., 1987. The goodness of fit to ideal Gauss and Rosin distributions: a new grain-size parameter. J. Sediment. Petrol. 57, 871–880.

Sparks, R.S.J., 1997. Causes and consequences of pressurisation in lava dome eruptions. Earth Planet. Sci. Lett. 150, 177–189.

Spieler, O., Kennedy, B., Kueppers, U., Dingwell, D.B., Scheu, B., Taddeucci, J., 2004. The fragmentation threshold of pyroclastic rocks. Earth Planet. Sci. Lett. 226, 139–148.

Taddeucci, J., Spieler, O., Kennedy, B., Pompilio, M., Dingwell, D.B., Scarlato, P., 2004. Experimental and analytical modelling of basaltic ash explosions at Mt. Etna, Italy, 2001. J. Geophys. Res. 109, B08203, doi:10.1029/2003JB002952.

Weiner, B.B., 1984. Particle and droplet sizing using Fraunhofer diffraction. In: Barth, H.G. (Ed.), Modern Methods of Particle Size Analysis. J. Wiley and Sons, New York.

Zimanowski, B., Wohletz, K., Dellino, P., Büttner, R., 2003. The volcanic ash problem. J. Volcanol. Geotherm. Res. 122, 1–5.